J Appl Electrochem (2010) 40:1651–1657
DOI 10.1007/s10800-010-0152-4

ORIGINAL PAPER

Direct electrochemistry of myoglobin immobilized in NiO/MWNTs hybrid nanocomposite for electrocatalytic detection of hydrogen peroxide

Jian-Ding Qiu · San-Guan Cui · Min-Qiang Deng · Ru-Ping Liang

Received: 20 November 2009 / Accepted: 18 May 2010 / Published online: 4 June 2010

Abstract A novel matrix, multiwalled carbon nanotubes supported nickel oxide nanoparticles composite nanomaterial (NiO@MWNTs), for immobilization of protein and biosensing was designed using a simple and effective hydrothermal method. Using myoglobin (Mb) as a model, the direct electrochemistry of immobilized Mb indicated the matrix could accelerate the electron transfer between protein's active sites and the electrode. The modified electrode shows excellent electrocatalytic activity toward the reduction of H_2O_2 without the help of an electron mediator. The simple operation, fast response, acceptable stability, and reproducibility of the proposed biosensor indicated its promising application in protein immobilization and preparation of the third generation biosensors.

Keywords Hydrothermal · NiO nanoparticle · Multiwalled carbon nanotubes · Myoglobin · Direct electrochemistry

1 Introduction

Direct electron transfer (DET) of redox proteins or enzymes has attracted great interest, because it provides not only a foundation for fabricating biosensors without addition of mediators [1–4], but also a good model for mechanistic studies of their electron transfer activity in the biological systems [5–7]. However, DET between the active site of the redox proteins and the underlying electrode surface is commonly forbidden. This is because proteins usually have big and complex structures where the redox centers deeply immerse in the bodies [8], and in addition the denaturation and loss of electrochemical activities will occur when the proteins adsorbed directly on the electrode surface [9, 10]. Thus, the development of suitable matrix for the entrapment of redox proteins in electrode surface is important for facilitating their electron transfer. Extensive efforts have been made to utilize nanomaterials to immobilize proteins for transducer surface fabrication. Among nanostructured metal oxides such as CeO_2 [11, 12], ZnO [13–15], ZrO_2 [16, 17], Al_2O_3 [18], TiO_2 [8], Fe_3O_4 [19], etc., NiO NPs [20–22] have recently been used for direct adsorption and interaction of desired proteins with NiO NPs due to their good biocompatibility and unique ability to promote faster electron transfer between electrode and active site of desired protein.

Recently, hybrid nanomaterials have drawn much attention by biosensor researchers because they not only show their unexpected combined properties of the original components, but also cause changes in optical, chemical, or other performances compared with those of the individual components. Various hybrid nanomaterials films such as TiO_2/MWNTs [23], Au NPs/CNTs [24, 25], and MWNTs-Fc [26] have been used to immobilize proteins or enzymes on electrode surface for either mechanistic study of the proteins or fabricating electrochemical biosensors. These hybrid nanomaterials exhibited desirable microenvironment for protein immobilization and great facilitation of the electron transfer compared with those of the individual components [27, 28]. Recently, NiO@CNTs hybrid nanobiocomposite was prepared by chemical precipitation

J.-D. Qiu (✉) · S.-G. Cui · M.-Q. Deng · R.-P. Liang
Department of Chemistry and Institute for Advanced Study, Nanchang University, Nanchang 330031, People's Republic of China
e-mail: jdqiu@ncu.edu.cn

J.-D. Qiu
Department of Chemical Engineering, Pingxiang College, Pingxiang 337055, People's Republic of China

method to improve the electrochemical capacitance properties of NiO NPs [29, 30]. However, no attempts have been made toward application of NiO@CNTs to protein DET.

In present work, a simple and effective hydrothermal method was developed to synthesize NiO@MWNTs hybrid nanobiocomposite, in which NiO NPs were homogeneously dispersed and tightly captured on the side wall of MWNTs. Based on the good biocompatibility, larger surface area, and excellent conductivity of the prepared hybrid nanomaterial, a three-dimensional porous biofilm electrode was constructed. Using myoglobin (Mb) as a model protein, the properties and the feasibility of the biosensor for fast electron transfer were investigated. The morphology and the electrochemistry of the nanocomposite film were imaged by TEM and electrochemical techniques. The results showed that the formation of NiO@MWNTs nanocomposite not only increased the Mb loading, retained the biological activity of the immobilized Mb efficiently, but also accelerated the electron transfer between electrode and active sites of the immobilized Mb. The prepared biosensor exhibited good analytical performances, indicating that NiO@MWNTs hybrid nanomaterial can be a good candidate to prepare biocompatible and conductive interface for protein immobilization and open a way for its application in direct electrochemistry of proteins without any electron transfer mediator.

2 Experimental procedures

2.1 Chemicals and reagents

MWNTs with diameters ranging from 10 to 20 nm and lengths ranging from 5 to 15 μm, were provided by Shenzhen Nanotech Port Co. Ltd and purified using literature techniques [31]. Mb from equine skeletal muscle (molecular weight, MW, 17,800) was purchased from Aldrich and used as received. H_2O_2 (30% w/w), $Ni(NO_3)_2$, $CO(NH_2)_2$, HNO_3, and other reagents used were of analytical grade and super pure water was used throughout.

2.2 Synthesis of the NiO@MWNTs nanocomposite

NiO@MWNTs nanocomposite was prepared according to Zheng's method with a little modification [29]. Briefly, 100 mg of the purified MWNTs were added into 15 mL of 1.25 mg mL^{-1} sodium dodecyl phenyl sulfate solution. After being ultrasonicated for 1.5 h, 15 mL of 0.2 M $Ni(NO_3)_2$ solution was mixed well with MWNTs suspension. 13 mL of 1 M $CO(NH_2)_2$ was then dropped into this suspension and the mixture was stirred at 90 °C for 4 h. The mixed solution was then transferred into a Teflon-lined stainless steel autoclave, sealed and maintained at 90 °C for 10 h. After cooling down quickly, a large amount of precipitate was obtained by filtration, washed with super pure water and absolute ethanol several times, respectively. The obtained products were dried at 105 °C for 10 h in vacuum, and then thermally decomposed at 300 °C for 3 h. Finally, 6 mg NiO@MWNTs nanocomposites were redispersed in 2.0 mL pH 7.0 PBS solution with ultrasonicating.

2.3 Preparation of Mb/NiO@MWNTs biofilm

Glassy carbon electrode (GCE, 3 mm in diameter) was wet polished on a polishing cloth with 1.0, 0.3, and 0.05 μm alumina powder, respectively, and rinsed thoroughly with super pure water between each polishing step. The electrode was successively sonicated in 1:1 nitric acid, ethanol, and super pure water, and then allowed to dry at room temperature. After mixing 0.5 mL of 5.0 mg mL^{-1} Mb solution (dissolved in 0.1 M pH 7.0 PBS) with 1.0 mL NiO@MWNTs suspension, 6 μL of the mixture was uniformly cast onto the well-polished GCE surface. The modified electrode was dried at 4 °C overnight. The obtained film was denoted as Mb/NiO@MWNTs. For comparison, Mb/MWNTs modified electrode without NiO NPs was also prepared using the same procedure. All the resulting electrodes were stored at 4 °C when not in use.

2.4 Apparatus and measurements

The surface morphologies of MWNTs and NiO@MWNTs were estimated by transmission electron microscopy (TEM, H600, Hitachi Instrument, Japan) at an accelerating voltage of 75 kV. The crystal structure of NiO@MWNTs nanocomposite was analyzed by X-ray diffraction (XRD) on a Rigaku powder diffractometer equipped with Cu $K\alpha_1$ radiation ($\lambda = 1.5406$ Å). UV–vis absorbance spectroscopy was performed using a UV-2550 spectrophotometer (Shimadzu). Electrochemical measurements were performed on an Autolab PGSTAT30 electrochemical workstation (Eco Chemie). A conventional three-electrode system was used including an Ag/AgCl reference electrode, a Pt wire counter electrode, and the modified electrode as the working electrode. The electrolyte solutions were purged with high-purity nitrogen for at least 15 min to remove oxygen and maintained under nitrogen atmosphere during measurements.

3 Results and discussion

3.1 Characterization of NiO@MWNTs nanocomposite

TEM was used to confirm the configuration of the NiO@MWNTs nanocomposite. Figure 1a shows the TEM

image of MWNTs before modification with NiO NPs. It can be seen that the diameter of MWNTs is 10–20 nm with a rather smooth surface. After hydrothermal treatment of MWNTs in $Ni(NO_3)_2$ and $CO(NH_2)_2$ aqueous solution, it can be clearly seen that the surface of MWNTs become roughened and lots of NiO NPs are spontaneously attached on the sidewalls of MWNTs in a selective manner (Fig. 1b). Also, it is interesting that almost all the NiO NPs preferentially adhere to the surfaces of MWNTs rather than to other regions without MWNTs. The process of the growth of NiO NPs on the sidewalls of MWNTs can be described as follows [30, 32]: the positively charged precursors of $Ni(NO_3)_2$ are electrostatically adsorbed onto the surface of negatively charged MWNTs. The MWNTs with high specific surface area can act as a template for a nucleation of the NiO, and furthermore the reflux and sonication process creates more defect sites on the MWNTs walls, thus creating more effective nucleation sites and later NiO NPs are spontaneously formed on the surface of MWNTs.

The purified MWNTs and the NiO@MWNTs nanocomposite were then analyzed using XRD, respectively. As shown in Fig. 2a, the pattern for MWNTs exhibited typical diffraction peaks at 26.03°, 42.89°, and 53.62° are observed and can be assigned to diffraction from the (002), (100), and (004) planes, which is in agreement with those for MWNTs [33]. For the NiO@MWNTs nanocomposite in Fig. 2b, besides the MWNTs peaks, five new diffraction peaks at 37.38°, 43.38°, 62.68°, 75.48°, and 79.48° corresponding to (111), (200), (220), (311), and (222) planes of NiO NPs are clearly observed (JCPDS card no. 44-1159). In addition, the characteristic peak of MWNTs (002) is weakening seriously, which mainly results from the coverage of MWNTs with NiO NPs. The XRD results are consistent with above TEM results, clearly demonstrating that NiO NPs are newly introduced on the surface of MWNTs and the NiO@MWNTs nanocomposite are successfully prepared by this simple hydrothermal treatment method.

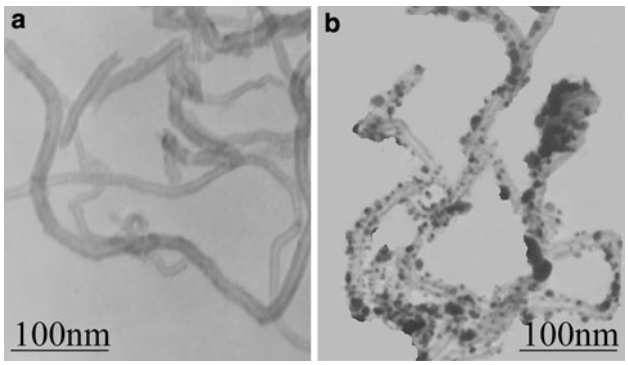

Fig. 1 TEM images of purified MWNTs (**a**) and NiO@MWNTs nanocomposite (**b**)

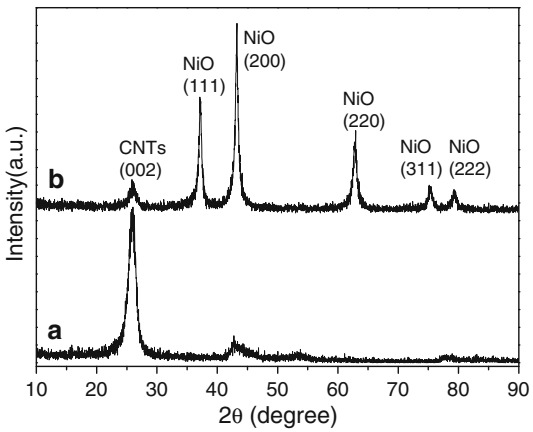

Fig. 2 XRD patterns of purified MWNTs (a) and NiO@MWNTs nanocomposite (b)

3.2 UV–Vis spectroscopic analysis

UV–Vis spectroscopy is a useful tool for monitoring the possible change of the Soret absorption band in the heme group region. The band shift may provide some information for possible denaturation in heme protein particularly that of conformational changes [34]. UV–Vis spectroscopy was thus carried out to investigate the structure of Mb immobilized in NiO@MWNTs nanocomposite film. As shown in Fig. 3, no prominent adsorption peak was obtained for NiO@MWNTs nanocomposite film (Fig. 3a). When Mb immobilized in NiO@MWNTs film, a new absorption peak at 411 nm was clearly observed (Fig. 3b), shifting only 1 nm toward the red in comparison with that of natural Mb in solution (Fig. 3c), indicated an interaction between NiO@MWNTs nanocomposite and Mb molecules. Such interaction did not change the fundamental microenvironment of Mb and the natural secondary structure of Mb immobilized in Mb/NiO@MWNTs biofilm was well retained.

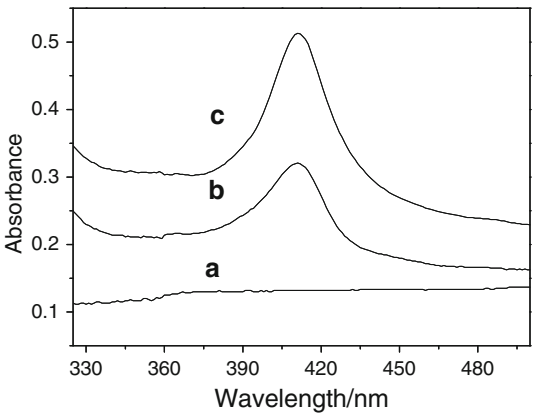

Fig. 3 UV–Vis spectra of NiO@MWNTs (a), Mb/NiO@MWNTs (b), and native Mb (c)

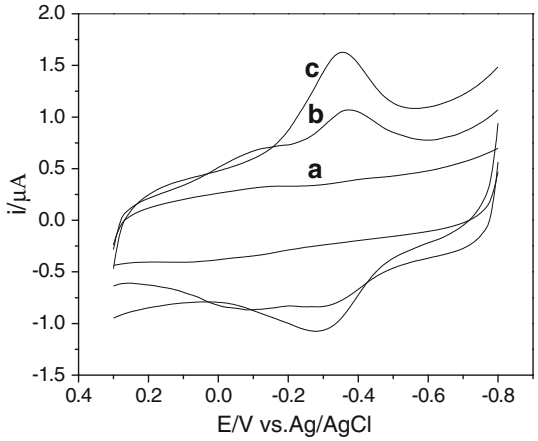

Fig. 4 CVs of NiO@MWNTs (a), Mb@MWNTs (b), and Mb/NiO@MWNTs (c) modified electrodes in 0.1 M PBS (pH = 7.0) at 100 mV s^{-1}

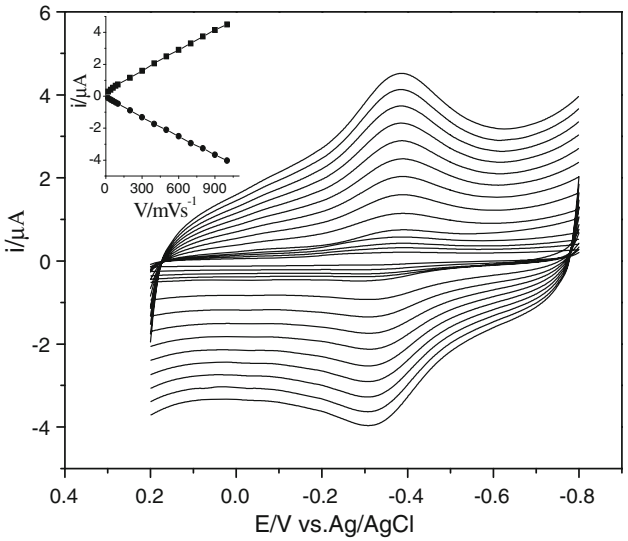

Fig. 5 CVs of Mb/NiO@MWNTs biofilm electrode in 0.1 M PBS (pH = 7.0) at various scan rate 20, 40, 60, 80, 100, 200, 300, 400, 500, 600, 700, 800, 900, and 1,000 mV s^{-1} (from inner to outer). *Inset*: plots of cathodic and anodic peak currents versus scan rate

3.3 Direct electrochemistry of the Mb/NiO@MWNTs biofilm

In order to investigate the electrochemical properties of different electrodes, cyclic voltammograms (CVs) were recorded at scan rate 100 mV s^{-1} in 0.1 M PBS solution (Fig. 4). No redox peaks were observed at the NiO@MWNTs electrode (Fig. 4a), and the redox peaks at the Mb@MWNTs electrode were small (Fig. 4b). In contrast, a pair of well-defined reduction–oxidation peaks with good stable and reproducibility was observed at the Mb/NiO@MWNTs electrode (Fig. 4c), which confirms that the redox peak pairs is correspondent to the real direct redox behavior of the immobilized Mb. The formal potential, the average of the anodic and cathodic peak potentials, was estimated to be −0.323 V. The cathodic and anodic peak currents were of similar magnitude, with a ratio about unity. The anodic peak potential and the cathodic peak potential of curve c in Fig. 4 were, respectively, −0.294 and −0.352 V with a small peak potential separation of 58 mV, which is similar to previous results [4, 35]. The observed DET from Mb could be due to the fact that the three-dimensional NiO@MWNTs nanocomposite film could provide multiple adsorption sites for Mb molecules, retaining the bioactivity of the adsorbed Mb. Thus, it is possible to achieve fast, DET between the heme site of immobilized Mb and the electrode surface.

The effect of scan rate on the response of the Mb/NiO@MWNTs electrode was shown in Fig. 5. With the increasing of scan rate from 20 to 1,000 mV s^{-1}, both the reduction and oxidation peaks currents (I_p) were increased linearly (Fig. 5 inset) and the peak to peak separation was 58 mV and nearly independent of the scan rate, which revealed that the electron transfer between Mb and GCE could be easily performed at the Mb/NiO@MWNTs biofilm and it was a surface-controlled process, not a diffusion-controlled process. According to the Laviron model $K_s = mnF_v/RT$ [36], the electron transfer rate constant (K_s) of Mb immobilized onto the Mb/NiO@MWNTs biofilm was estimated to be 2.65 s^{-1}, which is much higher than those of 0.93 s^{-1} for Mb immobilized on DL-homocysteine self-assembled gold electrode [37], 0.55 s^{-1} for Mb immobilized in clay–chitosan–gold nanoparticles modified glass carbon electrode [38], 0.34 s^{-1} for Mb entrapped in NiO nanoparticles modified glass carbon electrode [39], and close to 3.1 s^{-1} for Mb/CNT electrode [40]. Therefore, NiO@MWNTs nanocomposite may act as molecular wire, enhancing the DET of Mb providing a native environment for the protein molecules which is favorable for DET. The average surface coverage (Γ*) of Mb on the surface of Mb/NiO@MWNTs biofilm electrode was estimated to be 5.43×10^{-11} mol cm^{-2}, which is about 3.44 times of the theoretical monolayer coverage (1.58×10^{-11} mol cm^{-2}) of Mb [41], suggesting that several layers of Mb entrapped in the three-dimensional porous NiO@MWNTs nanocomposite film participated in the DET process. It is proposed that the presence of NiO@MWNTs nanocomposite provide a larger effective surface area available for protein binding and increase the loading of Mb.

3.4 Effect of pH on Mb/NiO@MWNTs biofilm electrode

CVs of Mb/NiO@MWNTs biofilm electrode were recorded in a series of PBS with the pH from 4.5 to 9.2 in the absence of oxygen (Fig. 6). It was found that nearly

reversible voltammograms can be observed for immobilized Mb in all the pH range tested from 4.5 to 9.2, with well defined and stable peaks. Both reduction and oxidation peak potentials of the Mb heme Fe(III)/Mb heme Fe(II) redox couple of Mb/NiO@MWNTs electrode are shifted negatively by increasing the pH. The pH dependences of the formal potential from pH 4.5 to 9.2 can be expressed as follows: $E^{\circ} = -0.0427\ \text{pH} - 0.0699$ ($R = 0.999$). The slope of -42.7 mV pH^{-1} was close to -48.7 mV pH^{-1} for Mb–clay films [42] and the expected value of -57.8 mV pH^{-1} for a reversible one-proton-coupled single electron transfer at 291 K [43]. The value of the slope was smaller than -57.8 mV pH^{-1} perhaps because of the influence of the protonation states of *trans* ligands to the heme iron and amino acids around the heme or to the protonation of the water molecule coordinated to the center that may exist in different states under different pH values [35]. Thus, the reaction mechanism for the electrochemical reduction of Mb might be described as follows [43]:

$$\text{MbFe(III)} + \text{H}^{+} + e^{-} \leftrightarrow \text{MbFe(II)}$$

3.5 Electrocatalysis of Mb/NiO@MWNTs biofilm to the reduction of H_2O_2

It was reported that proteins containing heme groups, such as HRP, cytochrome *c*, hemoglobin, Mb, and hemin, are capable to reduce H_2O_2 electrocatalytically [44]. Figure 7 shows the CVs of the Mb/NiO@MWNTs biofilm electrode in 0.1 M PBS (pH = 7.0) in the absence (curve a) and the presence of different concentrations of H_2O_2 (curves b–j) at a scan rate of 100 mV s^{-1}. In the absence of H_2O_2, a pair of the redox peaks of Mb was observed (Fig. 7a), which was the same as curve c in Fig. 4. By introducing H_2O_2 to the PBS solution, an increase in the reduction peak was observed with the decrease of the oxidation peak for Mb (Fig. 7b–j). The reduction peak current increased with the concentration of H_2O_2 in PBS solution, which could be employed to determine the H_2O_2 concentration. These results illustrated that Mb immobilized in the Mb/NiO@MWNTs biofilm retained its bioactivity and exhibited excellent electrocatalytic activity toward the reduction of H_2O_2. The electrocatalytic process can be expressed as follows [45]:

$$\text{ferric Mb} + \text{H}_2\text{O}_2 \rightarrow \text{Compound I} + \text{H}_2\text{O}$$

$$\text{Compound I} + \text{H}^{+} + \text{e}^{-} \rightarrow \text{Compound II}$$

$$\text{Compound II} + \text{H}^{+} + \text{e}^{-} \rightarrow \text{ferric Mb}$$

The amperometric response of the NiO@MWNTs, MWNTs, and Mb/NiO@MWNTs modified electrodes to H_2O_2 were recorded through successively adding H_2O_2 to a continuously stirred 0.1 M PBS (pH = 7.0) at an applied potential of -0.35 V (Fig. 8). When a large number of H_2O_2 were added to the PBS, the NiO@MWNTs (Fig. 8a) and MWNTs (Fig. 8b) film electrodes did not show discernible catalytic current. However, even a small amount of H_2O_2 was added, a stepwise growth of reduction current was significantly observed at Mb/NiO@MWNTs biofilm electrode (Fig. 8c). The current value achieved 95% of the steady state response within 7 s, indicating a fast response. The fast response can be mainly attributed to the fast diffusion process, good biocompatibility, and high electronic conductivity of the NiO@MWNTs nanocomposite. The Mb/NiO@MWNTs biofilm electrode showed a linear response to H_2O_2 concentration in the range from 1.0 to 182 μM, which was broader than 0.8–12.8 μM for Mb immobilized in zirconium phosphate nanosheets [46], 1.5–90 μM for Mb entrapped in colloidal gold NPs [47],

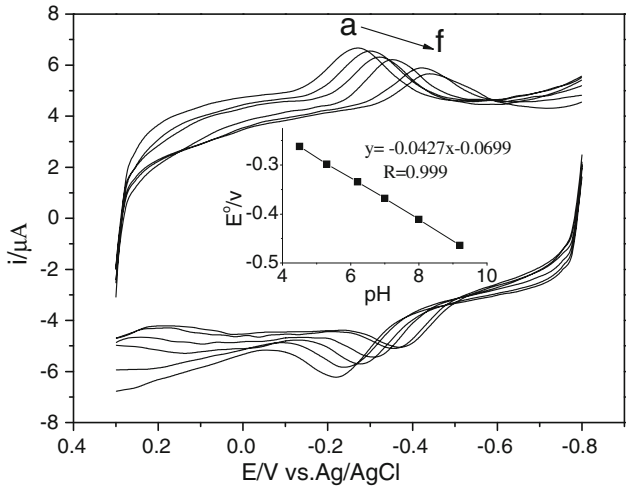

Fig. 6 CVs of Mb/NiO@MWNTs biofilm electrode in different pH solutions 4.5, 5.3, 6.2, 7.0, 8.0, and 9.2 (from a to f) at 100 mV s^{-1}. *Inset*: plot of formal potential versus pH

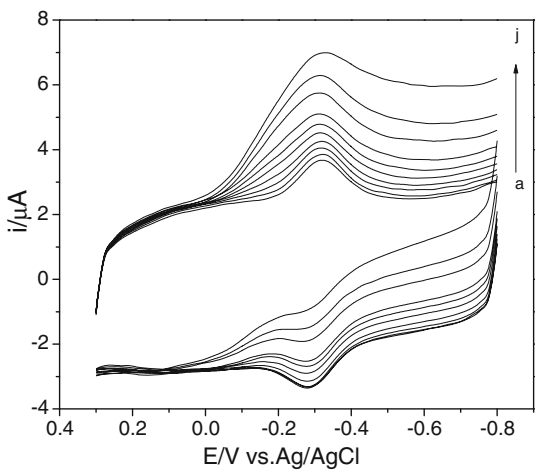

Fig. 7 CVs of Mb/NiO@MWNTs biofilm electrode in different concentrations of H_2O_2: 0, 5, 15, 30, 50, 70, 90, 130, 170, and 250 μM (from a to j) at 100 mV s^{-1}

1.0–125 μM at {SG-Al_2O_3/Mb}$_9$ film [48], and 0.5–90 μM at Mb/CNT [40]. A detection limit of 0.39 μM was obtained at S/N = 3, which was lower than those of 0.6 μM for Mb immobilized in [EMIM][BF4]-HA composite film [4] and 0.48 μM for Mb immobilized in gold NPs [49]. When H_2O_2 concentration was high, a response plateau was observed, showing the characteristics of the Michaelis–Menten kinetic mechanism. The apparent Michaelis–Menten constant (K_M), which gives an indication of the enzyme-substrate kinetics for the biosensor, can be obtained from the electrochemical version of the Lineweaver–Burk equation [50]:

$$1/I_{ss} = 1/I_{max} + K_M/I_{max}c$$

Here, I_{ss} is the steady state current after the addition of substrate, c is the bulk concentration of substrate, and I_{max} is the maximum current measured under saturated substrate solution. From the curve of the $1/I_{ss}$ versus $1/c$ based on the experimental data from Fig. 8, the K_M value of the biosensor was estimated to be 54.2 μM, which was much smaller than those of 140 μM for Mb immobilized in titanate nanotubes [51], 83.1 μM for Mb immobilized on TiO_2/MWNTs [23], and 1,300 μM for Mb entrapped in silver NPs [52]. The smaller value of K_M validates that the immobilized Mb on Mb/NiO@MWNTs biofilm possesses higher bioactivity and the proposed biosensor exhibits a higher affinity to H_2O_2.

3.6 Effects of interferences

The effect of potential interfering species such as dopamine, uric acid and ascorbic acid on the response of the present biosensor was evaluated in 0.1 M pH 7.0 PBS containing 30 μM H_2O_2 at the potential of −0.35 V. 0.1 mM dopamine, 0.1 mM uric acid, and 0.1 mM ascorbic acid generated a completely negligible increase in the biosensor response, demonstrating a good selectivity of the biosensor.

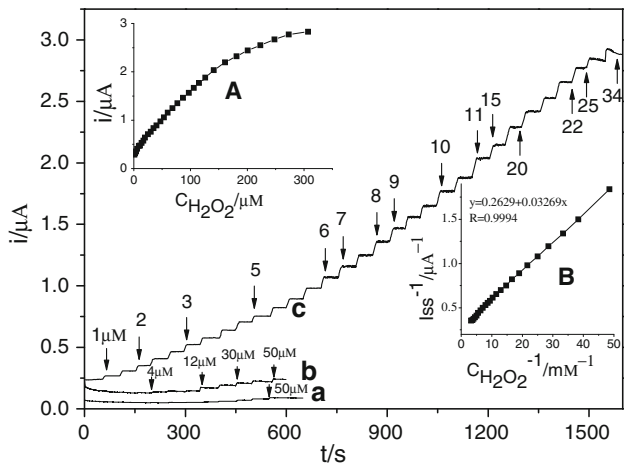

Fig. 8 Amperometric response of NiO@MWNTs (a), MWNTs (b), and Mb/NiO@MWNTs (c) modified electrodes at −0.35 V upon the successive addition of H_2O_2 in a stirred 0.1 M PBS (pH = 7.0). *Inset*: (A) calibration curve and (B) the Lineweaver–Burk plot

3.7 Stability and reproducibility of the Mb/NiO@MWNTs biofilm

The Mb/NiO@MWNTs biofilm electrode could retain the direct electrochemistry of the immobilized Mb at constant current value in 0.1 M PBS (pH = 7.0) upon the continuous CV sweep over the potential range from 0.3 to −0.8 V at 100 mV/s. After cyclically swept for 60 times the immobilized Mb changed only slightly of its initial activity. When the sensor was not in use, it was stored in 0.1 M PBS (pH = 7.0) at 4 °C. A storage period of a week almost did not change the current of the direct electrochemistry and the response to H_2O_2. The sensor could retain 92% of its initial response to H_2O_2 after 1 month. The fabrication of five electrodes, made independently, showed an acceptable reproducibility with the RSD of 1.2% for the current determination of 20 μM H_2O_2. The long-term stability and acceptable reproducibility of the biofilm can be attributed to that the presence of NiO@MWNTs can provide a favorable microenvironment for maintaining the bioactivity of the immobilized Mb and prevent the leakage of Mb.

4 Conclusion

In this work, a NiO@MWNTs hybrid nanocomposite was synthesized by a simple and effective hydrothermal method and first successfully applied in studying the immobilization and direct electrochemistry of Mb. The hybrid film prepared in this article provided high mechanical stability, larger surface area, biocompatible microenvironment, and particularly necessary conduction pathway to assist the DET of the Mb immobilized in the Mb/NiO@MWNTs biofilm. These advantages make the construction of biosensors simpler and the cost lower, and lead to fast DET behavior of the immobilized Mb and excellent performance of H_2O_2 detection. Thus, the NiO@MWNTs hybrid composite provided a good matrix for the further study on the DET of proteins and this strategy could be readily extended toward the preparation of the third generational biosensors and bioelectronics devices.

Acknowledgments We greatly appreciate the supports of the National Natural Science Foundation of China (20605010; 20865003; 20805023), the Jiangxi Province Natural Science Foundation (0620039; 2007JZH2644) and the Opening Foundation of State Key Laboratory of Chem/Biosensing and Chemometrics of Hunan University (2006022; 2007012).

References

1. Armstrong FA, Hill HAO, Walton NJ (1988) Acc Chem Res 21:407
2. Kong YT, Boopathi MN, Shim YB (2003) Biosens Bioelectron 19:227
3. Sun ZY, Li YQ, Zhou TS, Liu Y, Shi GY, Jin LT (2008) Talanta 74:1692
4. Zhang Y, Zheng JB (2008) Electrochem Commun 10:1400
5. Gorton L, Lindgren A, Larsson T, Munteanu FD, Ruzgas T, Gazaryan I (1999) Anal Chim Acta 400:91
6. Armstrong FA, Wilson GS (2000) Electrochim Acta 45:2623
7. Shumyantseva VV, Ivanov YD, Bistolas N, Scheller FW, Archakov AI, Wollenberger U (2004) Anal Chem 76:6046
8. Li Q, Luo G, Feng J (2001) Electroanalysis 13:359
9. Zhang W, Li G (2004) Anal Sci 20:603
10. Lu X, Wen Z, Li J (2006) Biomaterials 27:5740
11. Feng KJ, Yang YH, Wang ZJ, Jiang JH, Shen GL, Yu RQ (2006) Talanta 70:561
12. Saha S, Arya SK, Singh SP, Sreenivas K, Malhotra BD, Gupta V (2009) Biosens Bioelectron 24:2040
13. Deng Z, Tian Y, Yin X, Rui Q, Liu H, Luo Y (2008) Electrochem Commun 10:818
14. Zhu X, Yuri I, Gan X, Suzuki I, Li G (2007) Biosens Bioelectron 22:1600
15. Umar A, Rahman MM, Vaseem M, Hahn YB (2009) Electrochem Commun 11:118
16. Liu S, Dai Z, Chen H, Ju H (2004) Biosens Bioelectron 19:963
17. Zong S, Cao Y, Zhou Y, Ju H (2007) Biosens Bioelectron 22:1776
18. Yu J, Ma J, Zhao F, Zeng B (2007) Electrochim Acta 53:1995
19. Zhao G, Xu JJ, Chen HY (2006) Electrochem Commun 8:148
20. Salimi A, Sharifi E, Noorbakhsh A, Soltanian S (2006) Electrochem Commun 8:1499
21. Salimi A, Sharifi E, Noorbakhsh A, Soltanian S (2007) Biosens Bioelectron 22:3146
22. Salimi A, Sharifi E, Noorbakhsh A, Soltanian S (2007) Biophys Chem 125:540
23. Zhang L, Tia DB, Zhu JJ (2008) Bioelectrochemistry 74:157
24. Xiang C, Zou Y, Sun LX, Xu F (2007) Talanta 74:206
25. Wang Z, Li M, Su P, Zhang Y, Shen Y, Han D, Ivaska A, Niu L (2008) Electrochem Commun 10:306
26. Qiu JD, Zhou WM, Guo J, Wang R, Liang RP (2009) Anal Biochem 385:264
27. Besteman K, Lee JO, Wiertz FGM, Heering HA, Dekker C (2003) Nano Lett 3:727
28. Zhang Y, He PL, Hu NF (2004) Electrochim Acta 49:1981
29. Zheng Y, Zhang M, Gao P (2007) Mater Res Bull 42:1740
30. Lee JY, Liang K, An KH, Lee YH (2005) Synth Met 150:153
31. Tsang SC, Chen YK, Harris PJF, Green MLH (1994) Nature 372:159
32. Liu XM, Zhang XG, Fu SY (2006) Mater Res Bull 41:620
33. Kim HJ, Jeon KK, An KH, Kim C, Heo JG, Lim SC, Bae DJ, Lee YH (2003) Adv Mater 15:1757
34. George P, Hanania G (1953) Biochem J 55:236
35. Yamazaki I, Araiso T, Hayashi Y, Yamada H, Makino R (1978) Adv Biophys 11:249
36. Laviron E (1979) J Electroanal Chem 101:19
37. Zhang HM, Li NQ (2001) Bioelectrochemistry 53:97
38. Zhao X, Mai Z, Kang X, Dai Z, Zou X (2008) Electrochim Acta 53:4732
39. Moghaddam AB, Ganjali MR, Dinarvand R, Ahadi S, Saboury A (2008) Biophys Chem 134:25
40. Esplandiu MJ, Pacios M, Cyganek L, Bartroli J, Valle MD (2009) Nanotechnology 20:355502 (8 pp)
41. Liu HH, Tian ZQ, Lu ZX, Zhang ZL, Zhang M, Pang DW (2004) Biosens Bioelectron 20:294
42. Zhou YL, Hu NF, Zeng YH, Rusling JF (2002) Langmuir 18:211
43. Nassar AEF, Zhang Z, Hu N, Rusling JF, Kumosinski TF (1997) J Phys Chem B 101:2224
44. Wang Q, Lu G, Yang B (2004) Langmuir 20:1342
45. Tatsuma T, Mori H, Fujishima A (2000) Anal Chem 72:2919
46. Zhang Y, Chen X, Yang W (2008) Sens Actuators B 130:682
47. Yang W, Li Y, Bai Y, Sun C (2006) Sens Actuators B 115:42
48. Guo W, Lu H, Hu N (2006) Electrochim Acta 52:123
49. Zhang J, Oyama M (2005) J Electroanal Chem 577:273
50. Li J, Tan SN, Ge H (1996) Anal Chim Acta 335:137
51. Fan C, Pang J, Shen P, Li G, Zhu D (2002) Anal Sci 18:129
52. Gan X, Liu T, Zhong J, Liu X, Li G (2004) Chembiochem 5:1686